Designing One-Dimensional Covalent Organic Frameworks:

Novel Post-Synthetic Modification on Hydroxyl Groups and

Ratiometric Detection of Chemical Warfare Agent Mimics

Xiaoqin Shen, Bing Yan*

School of Chemical Science and Engineering, Tongji University, Siping Road 1239, Shanghai

200092, China.

1. Experimental section

* Corresponding author: Email address: byan@tongji.edu.cn (Bing Yan)

1.1. Materials

Tb(NO$_3$)$_3$·6H$_2$O was prepared by dissolving Tb$_2$O$_3$ into excess nitric acid with continuous magnetic stirring, followed by evaporation and crystallization several times. All the other solvents and reagents were obtained commercially and used without further purification. Deionized water was used throughout the experiments. Tetrakis(4-aminophenyl)ethene (ETTA) (97%), 2,6-diformylphenol (DFP) (97%), 4, 4', 4'', 4'''-(Pyrene-1,3,6,8-tetrayl) tetraaniline (PyTTA) (97%), 2,5-dihydroxyterephthalaldehyde (DHPA) (98%), 6,6'-bipicolinic acid (6, 6'-BA) (96%), 1-ethyl-(3-dimethylaminopropyl)carbonyldiimide hydrochloride (EDC·HCl) (97%), 4-(dimethylamino)pyridine (DMAP) (99%), 2-chloroethyl ethyl sulfide (2-CEES) (97%), diethyl cyanophosphonate (DCNP) (90%), methylphosphonic acid (MPA) (98%) diethylmethylphosphonate (DEMP) (97%), dimethylmethanephosphate (DMMP) (95%), triethyl phosphate (TEP) (99%), diethyl suffide (99%), 1-chlorobutane (99%), styrene (99%) were purchased from Adamas-beta. Acetone (99.5%), chloroform (CHCl$_3$) (99%), dichloromethane (DCM) (99.5%), ethyl acetate (EA) (99.5%), acetonitrile (MeCN) (99%), methanol (MeOH) (99.5%), tetrahydrofuran (THF) (99.5%), toluene (99.5%), 1,2-dichlorobenzene (o-DCB) (98%), n-hexane (97%), 1,4-dioxane (99.5%), N, N-dimethylformamide (DMF) (99.5%) and dimethyl sulfoxide (DMSO) (99.5%) were purchased from Greagent.

1.2. Instruments

The powder X-ray diffraction (PXRD) patterns were recorded on Bruker D8 ADVANCE diffractometer employing Cu Kα radiation (40 mA and 40 kV) with a 2θ

range from 5° to 40° at room temperature. The surface morphology and EDS analysis were performed on Hitachi S-4800 field emission scanning electron microscope (SEM) with a voltage of 5 kV-15 kV. Fourier transform infrared (FT-IR) spectra were obtained by a Nexus 912 AO446 infrared spectrum radiometer in the wavenumber range of 4000 - 400 cm^{-1}. X-ray photoelectron spectroscopy (XPS) spectra were noted under the ultrahigh vacuum (< 10^{-6} Pa) at pass energy (93.90 eV) with Axis Ultra DLD spectrometer (Kratos, Japan) by employing an Mg Kα (1253.6 eV) anode. Thermogravimetric (TG) curves were measured on a TA TGA 55 system operating at a heating rate of 10 °C/min in the range of 25 °C up to 700 °C under N_2 atmosphere. N_2 adsorption desorption measurements were carried out on a TRISTAR 3020. The element content of sample was determined using an inductively coupled plasma-optical emission spectrometer (ICP-OES). The fluorescence spectra were obtained on an Edinburgh FLS920 spectrophotometer employing 450 W xenon lamp as the source of excitation with appropriate cutoff filter. The Commission International de l'Eclairage (CIE) coordinate were calculated by CIE1931 chromaticity coordinate calculation according to the fluorescence emission spectra. The UV-vis absorption spectra were carried on an Agilent 8453 spectrometer. The pH values of aqueous solutions were determined by an INESA PHS-25 pH meter with an E-201F pH composite electrode, which was carefully calibrated by standard buffer solution before testing. The HOMO-LUMO orbital energies were optimized by the B3LYP hybrid density functional and the basis set was 6-31G (d).

1.3. Synthesis of PyTTADHPA-OH

PyTTA (11.3 mg, 0.02 mmol) and DHPA (6.6 mg, 0.04 mmol) were weighed into a 10 mL high-pressure flask with a vacuum valve, which were suspended in mesitylene (0.5 mL) and 1,4-dioxane (0.5 mL) with 0.1 mL of 6 M AcOH. After sonicated for 10 min, the tube was degassed by three freeze-pump-thaw cycles and sealed off. Upon warming to room temperature, the tube was placed in an oven at 120 ºC and left undisturbed for 72 h. The final product was collected by centrifugation washed with THF and acetone, and finally dried at 80 ºC under vacuum for 12 h

1.4. Luminescent sensing experiments

Different concentrations of 2-CEES or DCNP were dissolved in ethanol and Tb@ETTADFP-COOH (0.25 mg/2.0 mL) was added to the dispersion and soaked for 5 min. Using an FLS920 spectrometer, the emission intensities of fluorescence spectra were measured. Tb@ETTADFP-COOH samples for selectivity and anti-interference experiments were similarly prepared.

2. Supporting figures

a) Vesicants
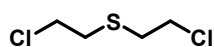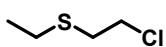
| Sulfur mustard (SM) | 2-Chloroethyl ethyl sulfide (2-CEES, half SM) | Bis(2-chloroethyl) ether (BCEE) | Nitrogen mustards (NM) |
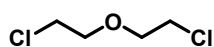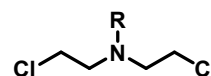
R = Me, Et, CH₂CH₂Cl
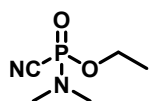
b) Nerve Agents
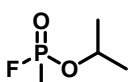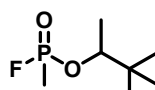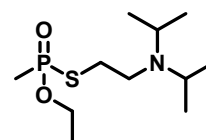
| Tabun | Sarin | Soman | VX |

c) Simulants
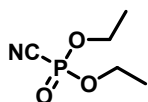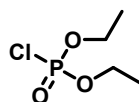
| Diethyl cyanophosphonate (DCNP) | Diethyl chlorophosphate (DCP) |

Scheme S1 Structure of various CWAs: a) vesicants, b) nerve agents and c) simulants of nerve agents.
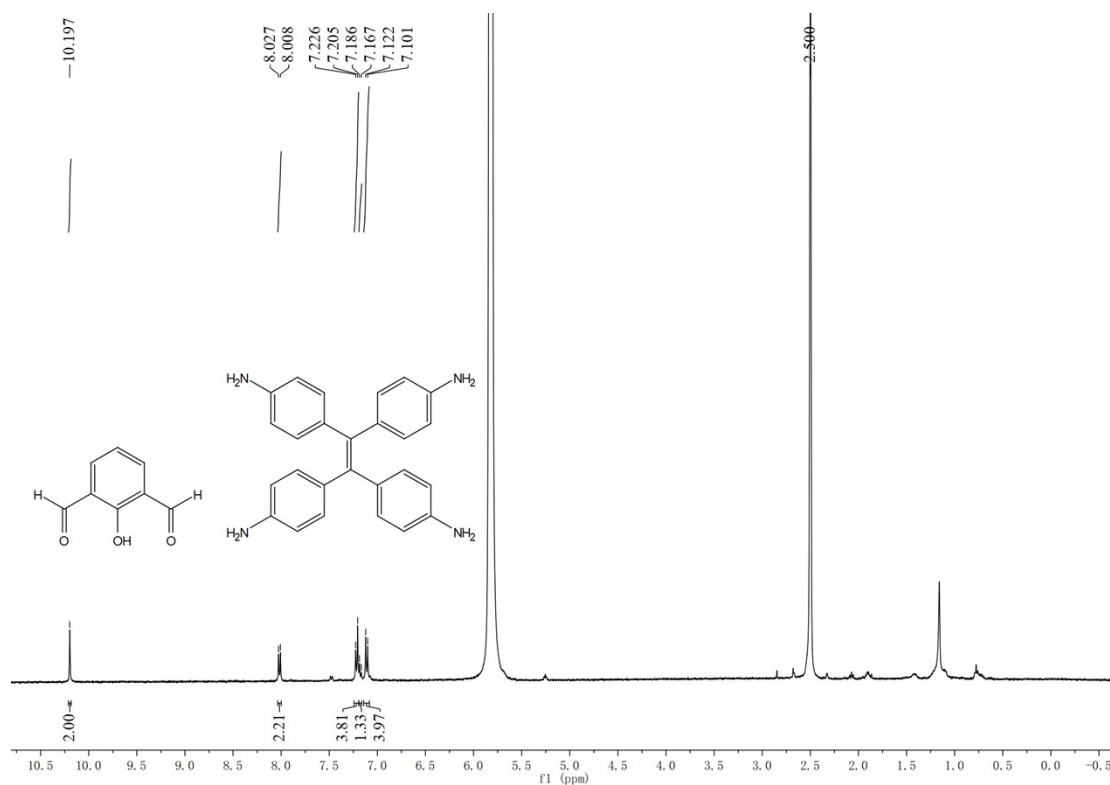
Fig. S1 ^{1}H NMR spectrum of digested ETTADFP-OH.
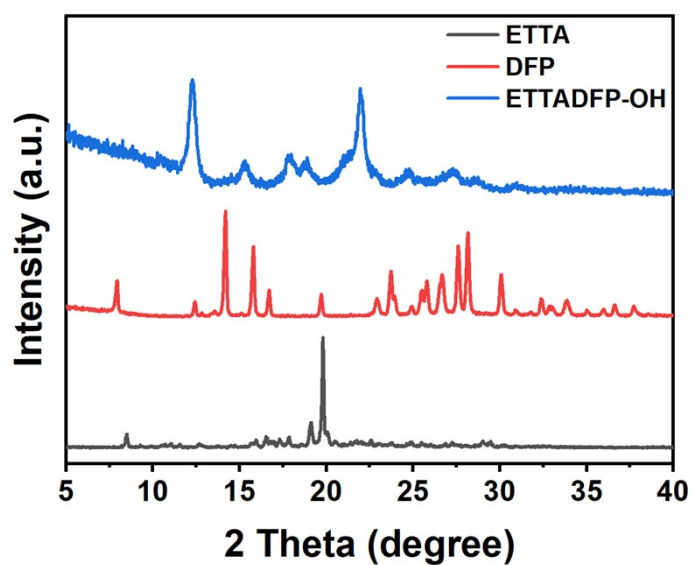
Fig. S2 PXRD patterns of ETTA, DFP and ETTADFP-OH.
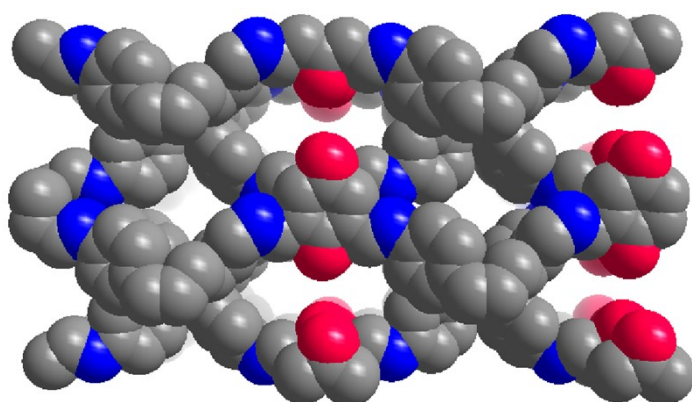
Fig. S3 AA stacking model of ETTADFP-OH.
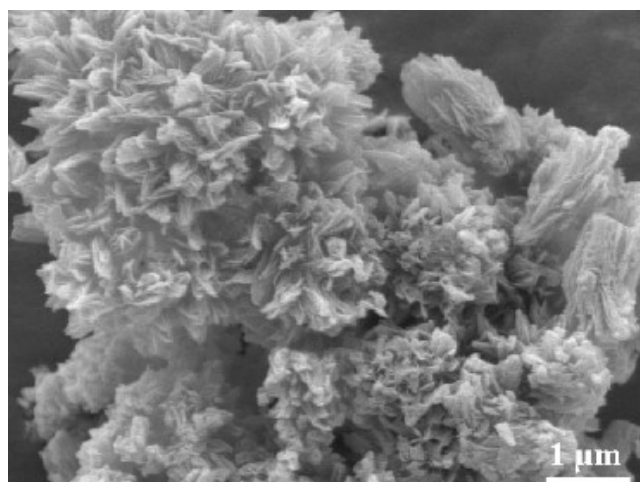
Fig. S4 SEM image of ETTADFP-OH.
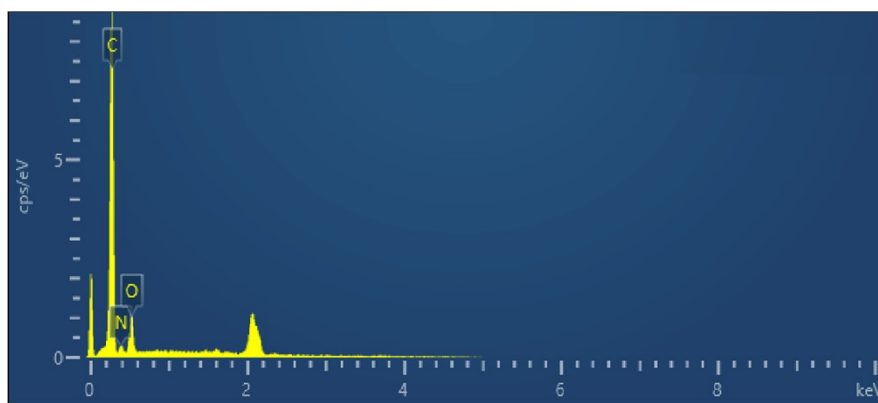
Element	Wt %	Wt % Sigma
C	79.37	1.14
N	7.20	1.11
O	13.43	0.68

Fig. S5 EDS analysis of ETTADFP-OH.
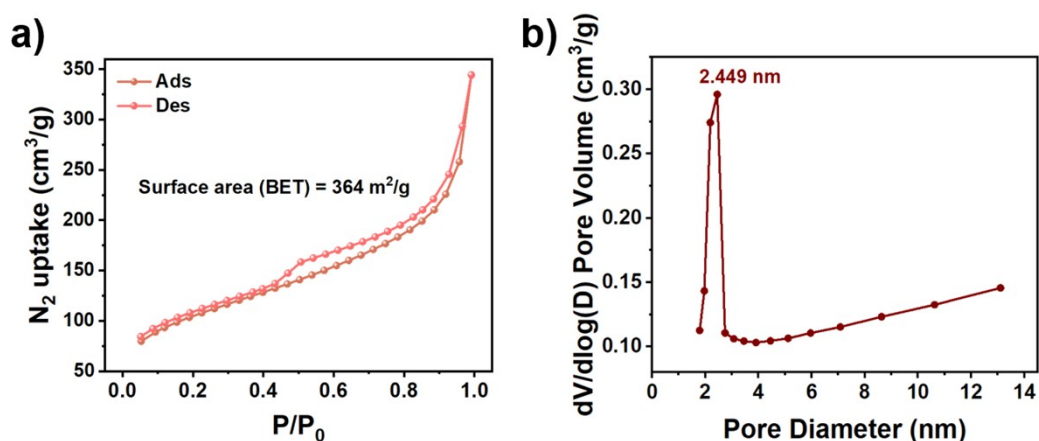
Fig. S6 a) N_2 adsorption–desorption isotherms of ETTADFP-OH. b) Pore size distribution of ETTADFP-OH.
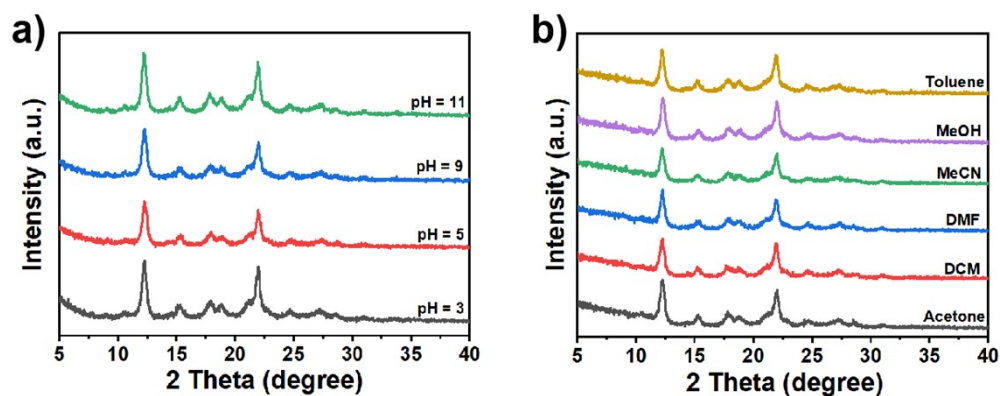
Fig. S7 PXRD patterns of ETTADFP-OH a) after soaking in different pH solutions for 48 h. b) after soaking in different organic solvents for 48 h.
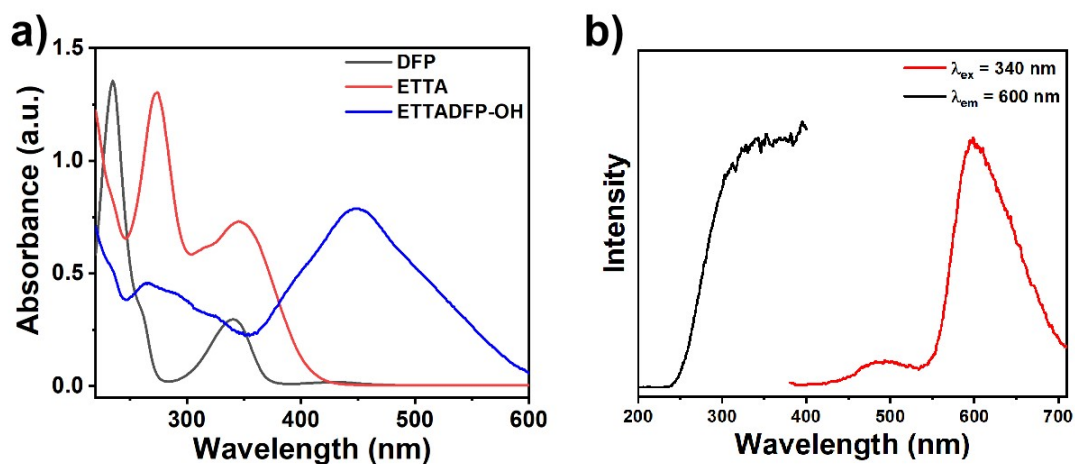
Fig. S8 a) UV-vis absorption spectra of DFP, ETTA and ETTADFP-OH. b) Excitation and emission spectra of ETTADFP-OH.
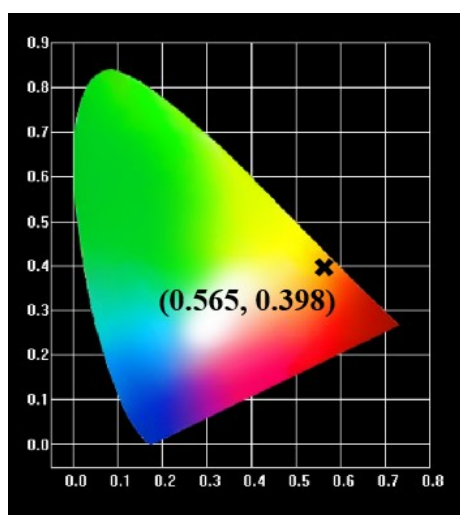
Fig. S9 The CIE coordinate of ETTADFP-OH.
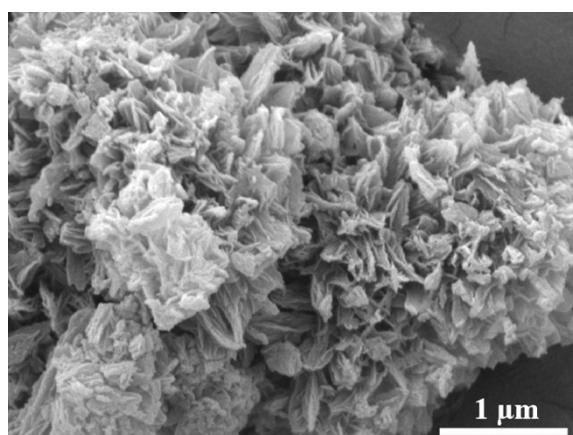
Fig. S10 SEM image of ETTADFP-COOH.
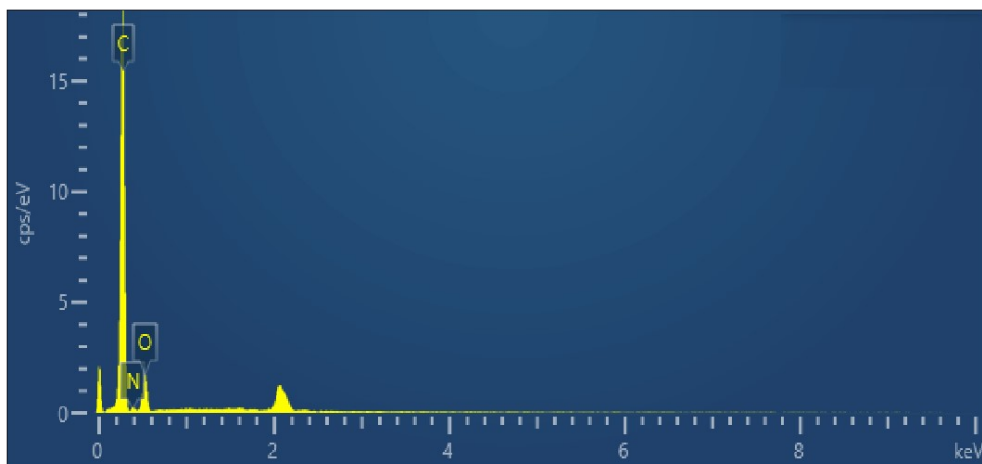
Element	Wt %	Wt % Sigma
C	76.70	0.90
N	5.82	0.95
O	17.48	0.52

Fig. S11 EDS analysis of ETTADFP-COOH.
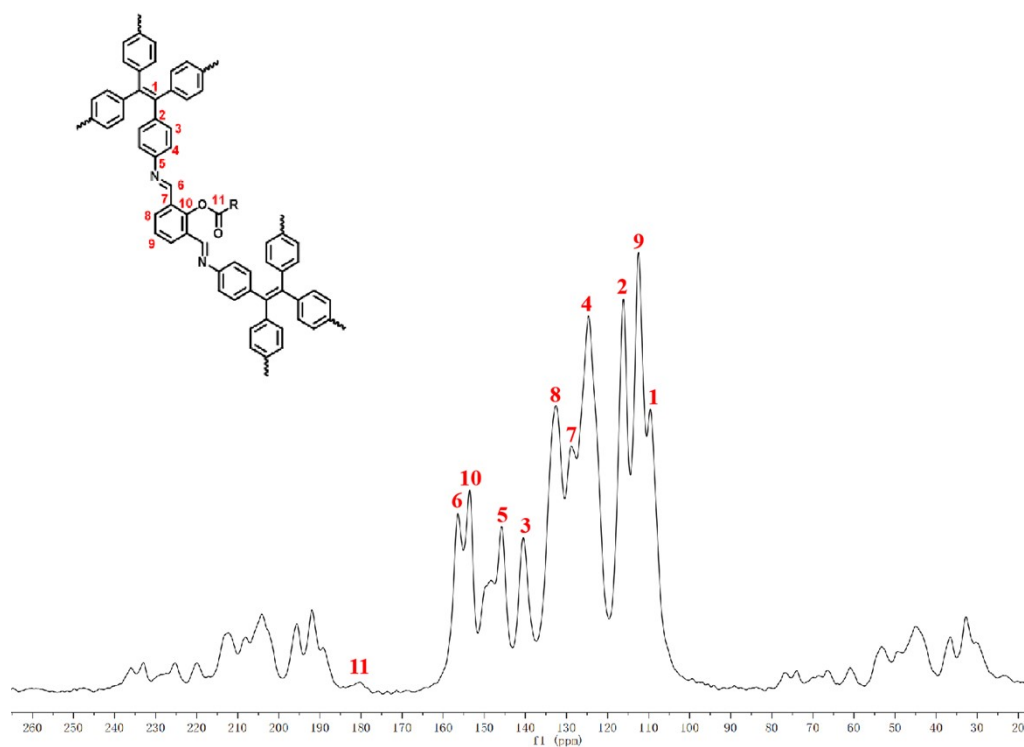
Fig. S12 ^{13}C CP/MAS solid-state NMR spectrum of and ETTADFP-COOH.
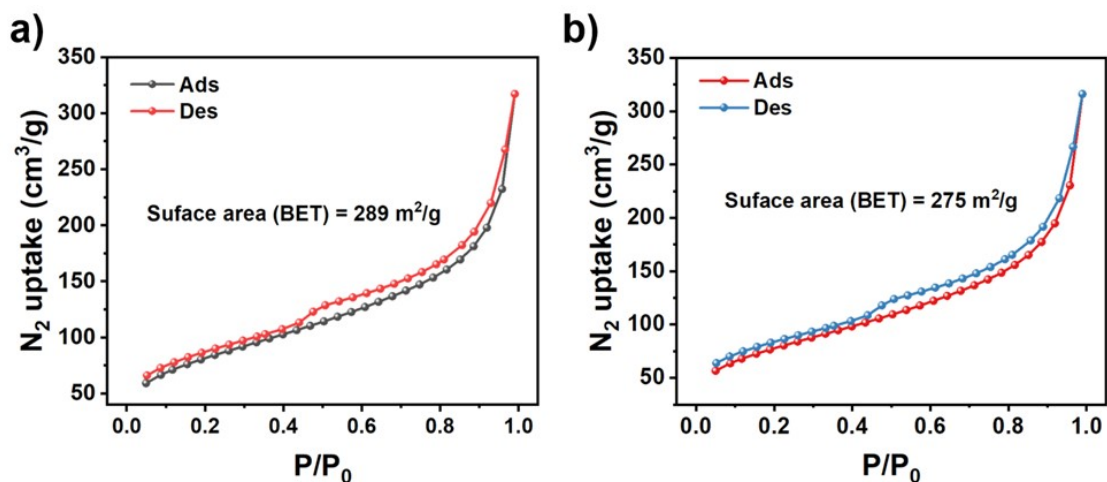
Fig. S13 a) N$_2$ adsorption–desorption isotherms of ETTADFP-COOH and b) N$_2$ adsorption–desorption isotherms Tb@ETTADFP-COOH.
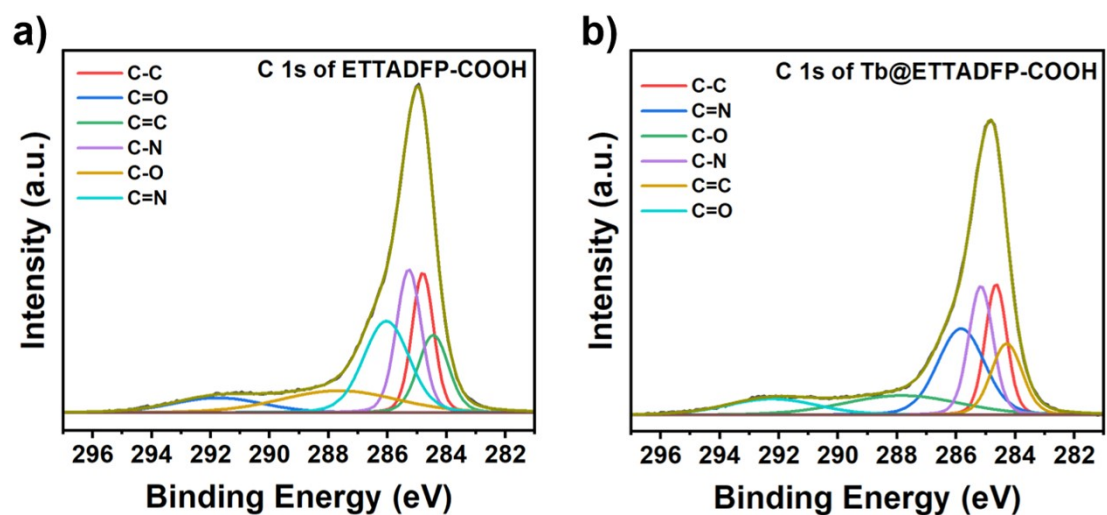
Fig. S14 XPS spectra of C 1s species in a) ETTADFP-COOH and b) Tb@ETTADFP-COOH.
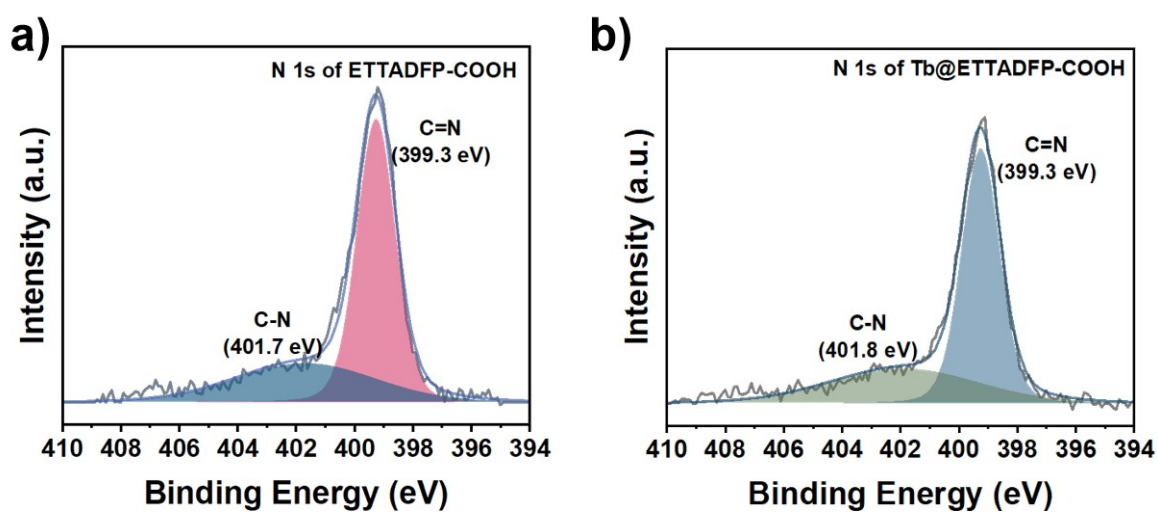
Fig S15 XPS spectra of N 1s species in a) ETTADFP-COOH and b) Tb@ETTADFP-COOH.
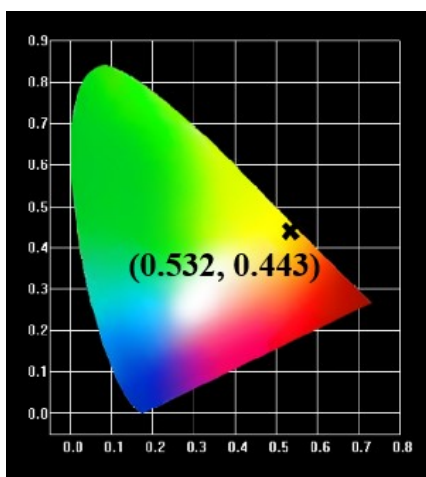
Fig. S16 The CIE coordinate of Tb@ETTADFP-COOH.
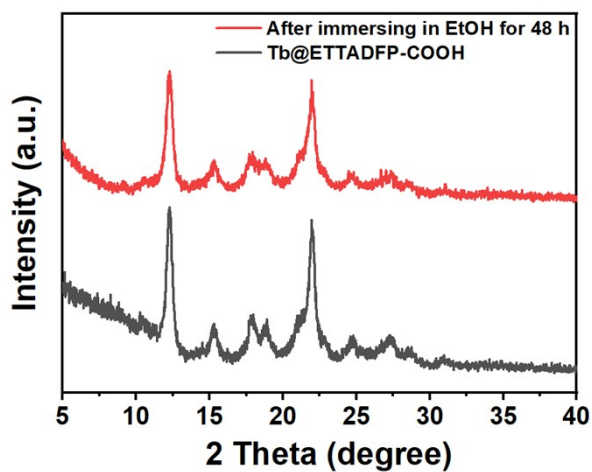
Fig. S17 PXRD pattern of Tb@ETTADFP-COOH before and after soaking in ethanol for 48 h.
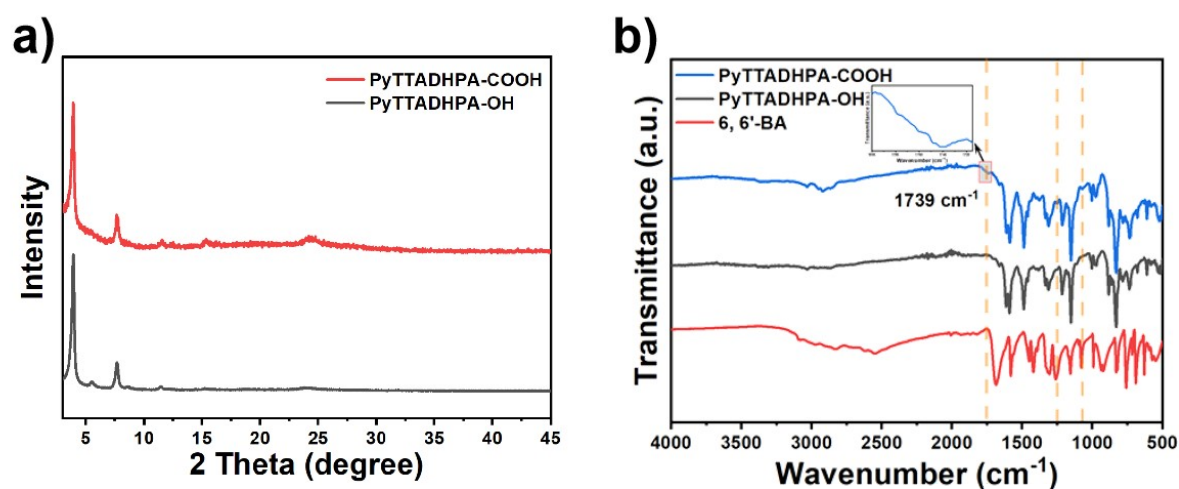
Fig. S18 a) PXRD patterns and b) FT-IR spectra of PyTTADHPA-OH and PyTTADHPA-COOH.
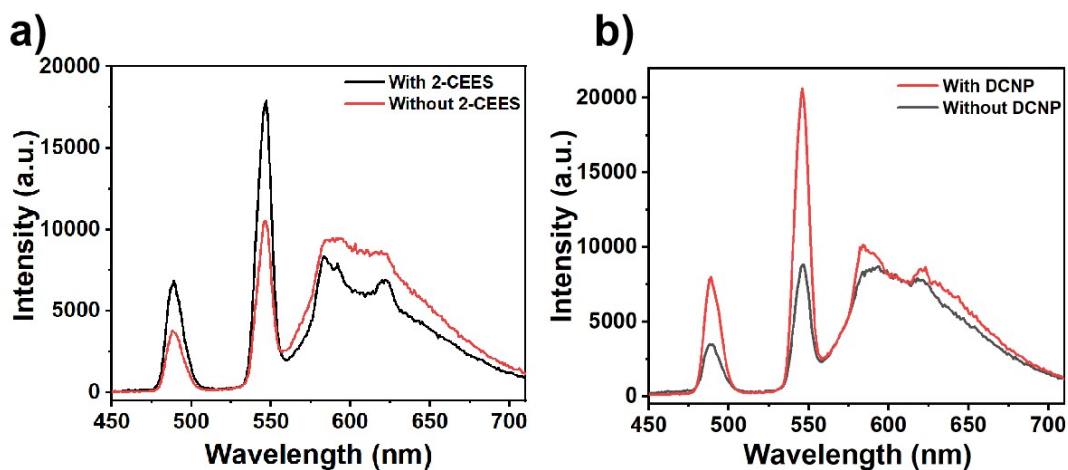
Fig. S19 The emission spectra of Tb@ETTADFP-COOH a) with and without 10^{-2} M 2-CEES b) with and without 10^{-2} M DCNP (λ_{ex} = 313 nm).
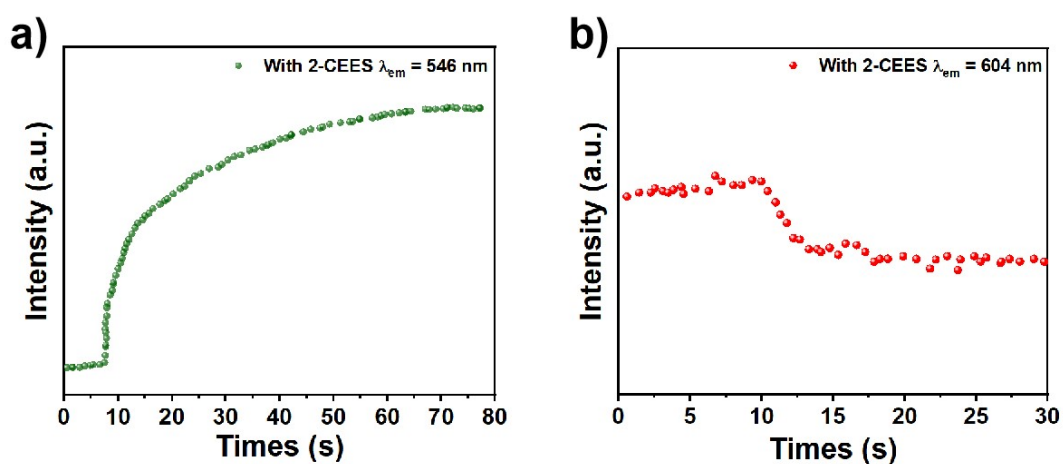
Fig. S20 Response time of Tb@ETTADFP-COOH to 2-CEES a) at 546 nm and b) at 604 nm.
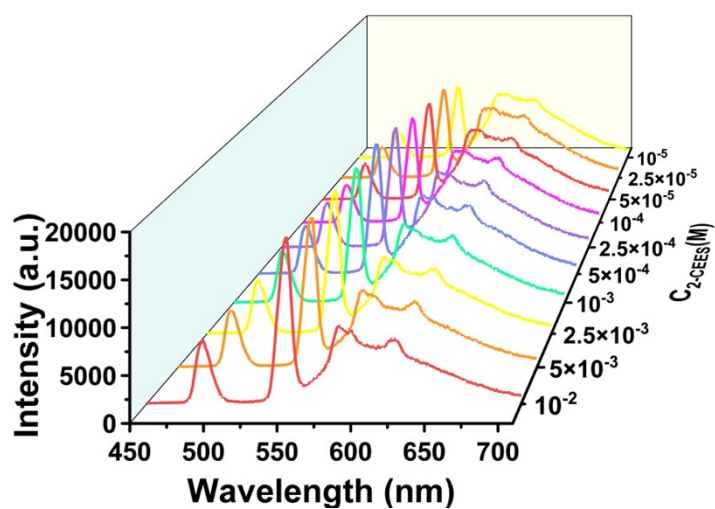
Fig. S21 The emission spectra of Tb@ETTADFP-COOH upon the gradual addition of 2-CEES.
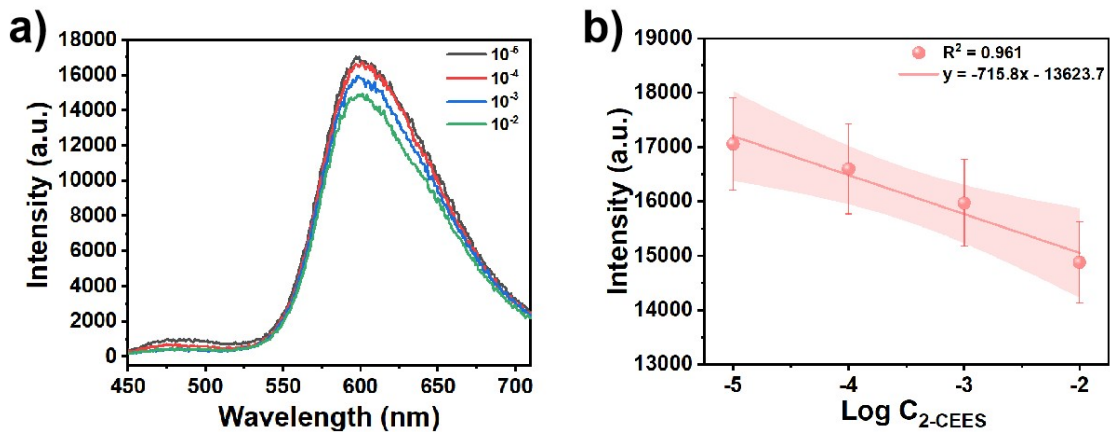
Fig. S22 a) Emission spectra of ETTADFP-OH in different concentrations of 2-CEES. b) Calibration curves of ETTADFP-OH toward 2-CEES (10^{-5} - 10^{-2} M)
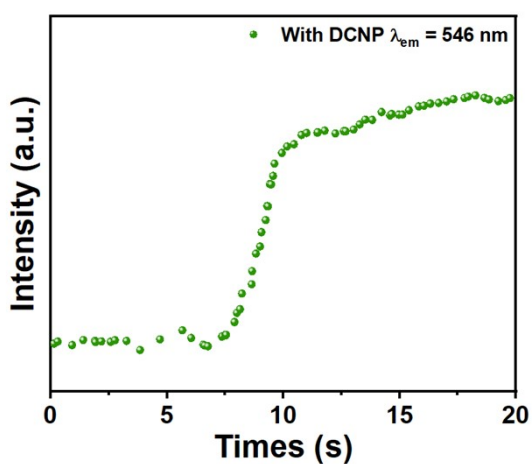
Fig. S23 Response time of Tb@ETTADFP-COOH to DCNP at 546 nm.
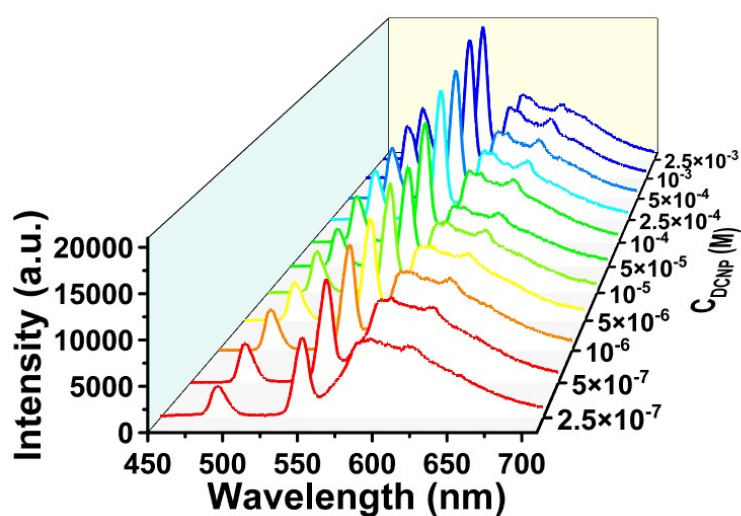
Fig. S24 The emission spectra of Tb@ETTADFP-COOH upon the gradual addition of DCNP.
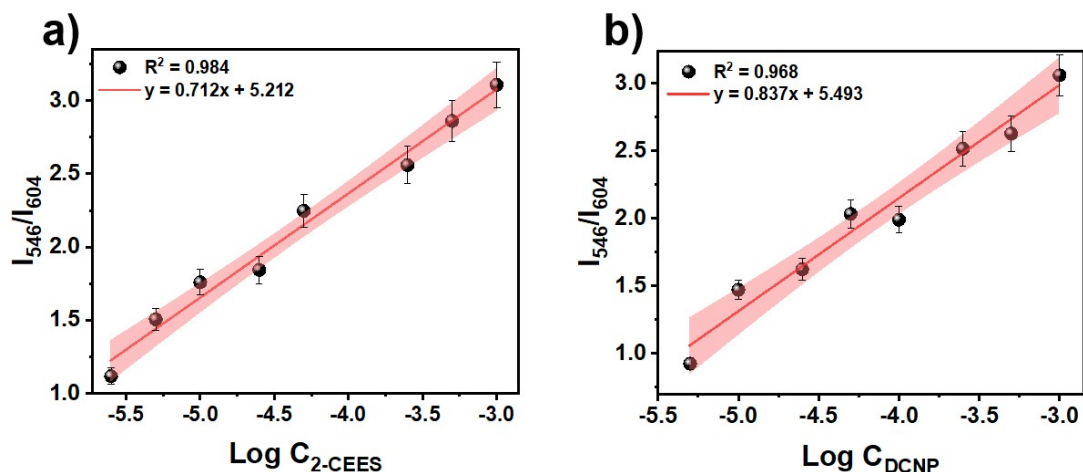
Fig. S25 Calibration curves of Tb@ETTADFP-COOH toward a) 2-CEES ($2.5×10^{-6}$ - 10^{-3} M) in river water. b) DCNP ($5×10^{-6}$ - 10^{-3} M) in river water.
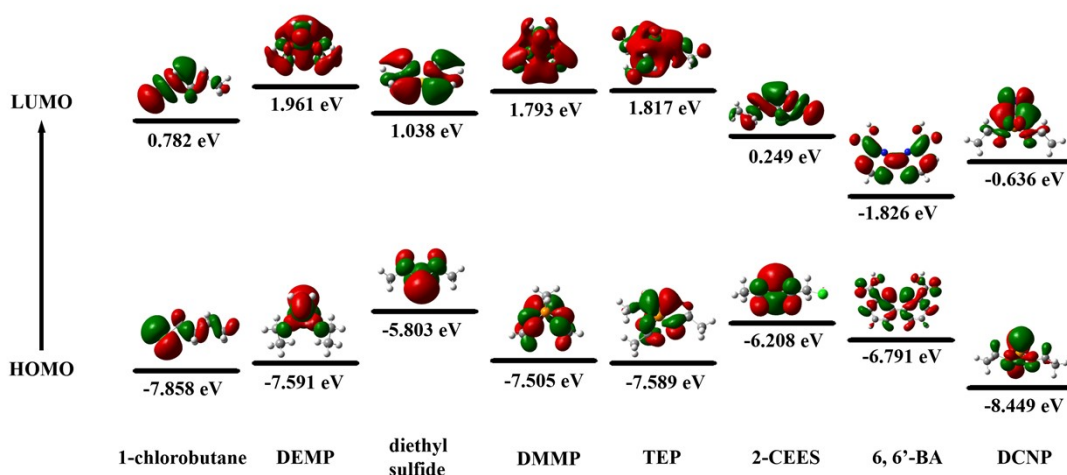
Fig. S26 LUMO and HOMO energy levels of Tb@ETTADFP-COOH, 2-CEES and DCNP.

Table S1. ICP-OES results of Tb@ETTADFP-COOH.

Sample	m_0 (g)	V_0 (mL)	Test element	C_0 (mg/L)	C_1 (mg/L)	C_x (mg/kg)	W (%)
Tb@ETTADFP-COOH	0.0263	25	Tb	18.384	18.384	17475.29	1.75

Table S2. Summary of the methods for sensing 2-CEES and DCNP.

Analyte	Method	Linear range/μM	LOD/μM	Ref
2-CEES	Fluorescence	0–200	10	[S1]
	Fluorescence	0-140	4.75	[S2]
	Fluorescence	0-600	1.2	[S3]
	Fluorescence	0-2000	3.0	[S4]
	Fluorescence	80-400	4.4	[S5]
	Fluorescence	10-10000	0.961	This method
DCNP	Fluorescence	0-120	0.02575	[S6]
	Fluorescence	0-80	0.034	[S7]
	Colorimetric Detection	0-1308	16.8	[S8]
	Fluorescence	0-1500	2.9	[S9]
	Fluorescence	1.96-7.83	0.186	[S10]
	Fluorescence	0.25–2500	0.0249	This method

References

[S1] V. Kumar and E. V. Anslyn, *Chem. Sci.*, 2013, **4**, 4292-4297.

[S2] D. Raghavender Goud, A. K. Purohit, V. Tak, D. K. Dubey, P. Kumar and D. Pardasani, *Chem. Commun.*, 2014, **50**, 12363-12366.

[S3] Y. Zhang, Y. Lv, X. Wang, A. Peng, K. Zhang, X. Jie, J. Huang and Z. Tian, *Anal. Chem.*, 2018, **90**, 5481-5488.

[S4] D. Li, H. Xi, S. Han and S. Zhao, *Anal. Methods*, 2021, **13**, 484-490.

[S5] P. Zheng, W. Cao, Y. Zhang, F. Li and M. Zhang, *ACS Sens.*, 2022, **7**, 1946-1957.

[S6] N. Dey, J. Kulhánek, F. Bureš and S. Bhattacharya, *J. Org. Chem.*, 2021, **86**, 14663-14671.

[S7] S. Li, Y. Zheng, X. Zhu, H. Wang, L. Liang, X. Wang, L. Yuan, F. Zhang, H. Zheng and C. Zhao, *Sens. Actuators, B*, 2021, **337**, 129804.

[S8] S. Xiao, M. Yuan, Y. Shi, M. Wang, H. Li, L. Zhang and J. Qiu, *Anal. Chim. Acta*, 2023, **1278**, 341706.

[S9] T. Sultana, M. Mahato, N. Tohora, S. Ahamed, P. Pramanik, S. Ghanta and S. Kumar Das, *J. Photochem. Photobiol., A*, 2023, **439**, 114584.

[S10] S. Thakur, J. Rohilla, K. Kumar, H. Kumar, R. Singh, V. Kaur, R. Kamboj and R. Kaur, *Analyst*, 2023, **148**, 2582-2593.